Clim Dyn (2010) 34:661–668
DOI 10.1007/s00382-008-0521-4

Sensitivity of North Atlantic subpolar gyre and overturning to stratification-dependent mixing: response to global warming

Ben Marzeion · Anders Levermann · Juliette Mignot

Received: 9 September 2008 / Accepted: 17 December 2008 / Published online: 10 January 2009

Abstract We use a reduced complexity climate model with a three-dimensional ocean component and realistic topography to investigate the effect of stratification-dependent mixing on the sensitivity of the North Atlantic subpolar gyre (SPG), and the Atlantic meridional overturning circulation (AMOC), to idealized CO_2 increase and peaking scenarios. The vertical diffusivity of the ocean interior is parameterized as $\kappa \sim N^{-\alpha}$, where N is the local buoyancy frequency. For all parameter values $0 \leq \alpha \leq 3$, we find the SPG, and subsequently the AMOC, to weaken in response to increasing CO_2 concentrations. The weakening is significantly stronger for $\alpha \geq \alpha_{cr} \approx 1.5$. Depending on the value of α, two separate model states develop. These states remain different after the CO_2 concentration is stabilized, and in some cases even after the CO_2 concentration has been decreased again to the pre-industrial level. This behaviour is explained by a positive feedback between stratification and mixing anomalies in the Nordic Seas, causing a persistent weakening of the SPG.

Keywords Subpolar gyre · Global warming · Ocean mixing · Atlantic overturning

B. Marzeion (✉)
EAPS, Massachusetts Institute of Technology,
Cambridge, MA, USA
e-mail: ben.marzeion@uibk.ac.at

B. Marzeion
Nansen Environmental and Remote Sensing Center and Bjerknes Centre for Climate Research, Bergen, Norway

Present Address:
B. Marzeion
Tropical Glaciology Group, Institute of Geography,
University of Innsbruck, Innsbruck, Austria

A. Levermann
Earth System Analysis, Potsdam Institute for Climate Impact Research and Institute of Physics,
Potsdam University, Potsdam, Germany

J. Mignot
LOCEAN, Université Pierre et Marie Curie, Paris, France

1 Introduction

The state of the climate system in the North Atlantic depends on the states of a number of coupled sub-systems, e.g. the subpolar gyre (SPG), the overflows over the Greenland–Scotland Ridge (GSR), and the AMOC (Drange et al. 2005). In particular, the AMOC is thought to contribute to the relatively warm European climate by transporting $\sim$1 PW of heat from the tropics northward (Hall and Bryden 1982; Ganachaud and Wunsch 2000; Trenberth and Caron 2001). While the strength of the AMOC is likely to influence global climate, e.g. by modulating the El Niño/Southern Oscillation phenomenom (Timmermann et al. 2005), the position of the Intertropical Convergence Zone (Vellinga and Wood 2002), and by changing North Atlantic surface elevation (Levermann et al. 2005), the strongest effects can be found in the northern North Atlantic. Changes in the North Atlantic flow patterns are important factors for the heat transport into the Nordic region (Hátún et al. 2005), and economically relevant for fisheries (Hátún et al. 2007). Model results suggest that the influence of increased greenhouse-gas concentrations will weaken the future AMOC, by causing decreased heat loss and increased freshwater input in the high latitudes, thus lowering the density of the surface water in the northern sinking regions (e.g. Manabe and

Stouffer 1994; Rahmstorf and Ganopolski 1999; Gregory et al. 2005).

On long timescales, the AMOC is strongly influenced by the rate of low latitude vertical diffusion (Munk and Wunsch 1998). While some current climate models employ parameterizations for vertical diffusion that take into account bottom roughness and surface conditions (e.g. Gnanadesikan et al. 2006; Jungclaus et al. 2006b), most models prescribe diffusivities that are constant in space and/or time in the ocean interior. The fact that diffusion may be influenced by stratification (Gargett and Holloway 1984) is thus usually not taken into account. Nilsson and Walin (2001) and Nilsson et al. (2003) argued that a reduction of high latitude surface water density will eventually lead to reduced stratification in a one-hemisphere ocean, which in turn could lead to increased mixing, and an increased AMOC. Similar results were found in a box model by Marzeion and Drange (2006). Saenko (2006) investigated the responce of the AMOC to the spatial distribution of energy available for mixing. While all these studies focused on the role of low latitude mixing for the stability of the AMOC, Marzeion et al. (2007) showed that high latitude mixing may be critical in controlling the vertical propagation of buoyancy anomalies imposed at the surface, and thereby influence stratification and circulation in the Nordic Seas.

Here, we test the sensitivity of the AMOC to increasing levels of atmospheric CO_2, and to reducing the CO_2 level back to pre-industrial values with varying delay using the same model as Marzeion et al. (2007), employing stratification-dependent vertical diffusivity in the ocean. The model and two sets of experiments are presented in the following section. The results for the CO_2 increase experiments are shown in Sect. 3, followed by the results of the CO_2 peaking experiments in Sect. 4. Finally, we discuss the results and conclude in Sect. 5.

2 Model and experiments

2.1 Model description

The global coupled climate model CLIMBER-3α (Montoya et al. 2005) combines a 3-dimensional ocean general circulation model based on the GFDL MOM-3 code with a statistical-dynamical atmosphere model (Petoukhov et al. 2000) and a dynamic and thermodynamic sea-ice model (Fichefet and Maqueda 1997). The oceanic horizontal resolution is 3.75° × 3.75°, and there are 24 vertical levels. The advection-diffusion scheme of Prather (1986) is applied to reduce numerical diffusion (Hofmann and Maqueda 2006).

The atmospheric component has a resolution of 7.5° in latitude and 22.5° in longitude and is assuming a universial vertical structure of temperature and humidity. Heat and freshwater fluxes between ocean and atmosphere are computed on the ocean grid, without any flux adjustment. The atmospheric grid is too coarse to be used for the wind forcing, we therefor use the NCEP/NCAR reanalysis wind stress climatology for the momentum flux.

2.2 Experimental setup

2.2.1 *Paramterization of vertical mixing*

For this study, the vertical diffusivity κ is parameterized as

$$\kappa = \kappa_0 \left(\frac{N}{N_0} \right)^{-\alpha}$$

where $\kappa_0 = 0.2 \times 10^{-4}\ \mathrm{m}^2\ \mathrm{s}^{-1}$, $N = \left(-\frac{g}{\rho_0} \frac{\partial \rho}{\partial z} \right)^{1/2}$ the local buoyancy frequency, with g being the gravity acceleration, ρ_0 being a reference density, and $\frac{\partial \rho}{\partial z}$ being the vertical density gradient. $N_0 = 7.3 \times 10^{-3}\ \mathrm{s}^{-1}$ is a typical value of N at pycnocline depth in the model, ensuring comparable values of the diffusivity κ at pycnocline depth independent of the choice of the parameter α.

The diffusivity is thus increasing with decreasing stratification, with the parameter α controlling the sensitivity of the mixing to changes in stratification (note that $\alpha = 2$ is a special case, since it implies that the energy available for mixing is held constant). Since values of α between 0 and 3 have been identified in measurements in the ocean (Sarmiento et al. 1976; Hoffert and Broecker 1978; Gargett and Holloway 1984; Rehmann and Duda 2000), we choose different values from this range in our experiments. Depending on the value of α, this parameterization results in $0.05 \times 10^{-4} \mathrm{m}^2\ \mathrm{s}^{-1} \lesssim \kappa \lesssim 0.3 \times 10^{-4}\ \mathrm{m}^2\ \mathrm{s}^{-1}$ in the global ocean around pycnocline depth in the equilibrium runs. In the deep ocean, where the stratification is weak, values of κ exceed $1.5 \times 10^{-4}\ \mathrm{m}^2\ \mathrm{s}^{-1}$ for $\alpha = 3$. A more detailed discussion regarding the mixing parameterization in this model can be found in Marzeion et al. (2007).

First, equilibrium runs of ~2,000 years are integrated with constant preindustrial CO_2 concentration of 280 ppm for different values of α. The equilibrium states of the AMOC are very similar for all values of α, except for $\alpha = 1.5$ and 2.5, where the AMOC is ~1 Sv weaker than in the other cases (Fig. 1). This is caused by a difference in the SPG strength, and will be discussed in Sect. 5.

2.2.2 *CO_2 increase experiments*

Starting from equilibrium, the atmospheric CO_2 concentration is increased with a rate of 1% year^{-1} up to 1,120 ppm (= 4 × 280 ppm) where it is stabilized after 140 year of integration (Fig. 1). The model was then integrated for another ~1,000 years for all values of α, and

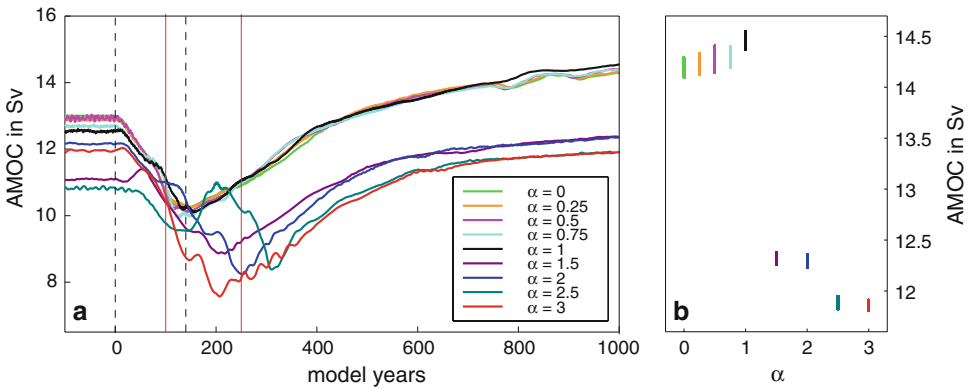

Fig. 1 **a** Time series of the maximum of the overturning stream function in the Atlantic for the CO_2 increase experiments. The *vertical black dashed lines* indicate the beginning and end of the CO_2 increase, the *vertical red lines* the times at which the values in Figs. 4 and 5 are taken. **b** Maximum of the overturning stream function in the Atlantic during years 900–1,000 as a function of α

for another $\sim$2,000 years for $\alpha = 0, 0.25, 0.5, 0.75, 1.5, 2.5$ (not shown).

2.2.3 CO_2 peaking experiments

Additionally, CO_2 peaking experiments are conducted for $\alpha = 1$ and $\alpha = 2$ by branching off of the CO_2 increase experiments. In these CO_2 peaking experiments, the atmospheric CO_2 concentration is reduced back to pre-industrial values at a rate of -1% year^{-1}. For $\alpha = 2$, the reduction is started every 25 years between 100 and 250 years after the increase was started (i.e. seven experiments for $\alpha = 2$). For $\alpha = 1$, only two CO_2 peaking experiments are conducted, starting the CO_2 reduction 150 and 250 years after the CO_2 increase was started.

This setup implies that in some of the CO_2 peaking experiments, the fourfold pre-industrial values of 1,120 ppm CO_2 is not reached before the reduction begins (see Fig. 2a, red dashed lines). After the pre-industrial values of CO_2 had been reached, the model was integrated for another $\sim$1,000 years with fixed CO2 concentrations.

3 Response to CO_2 increase

In response to CO_2 increase, the AMOC weakens in all experiments. A recovery sets in around the time of stabilization of the CO_2 concentration (between years $\sim$150 and $\sim$250 depending on α, see Fig. 1). Two different model states remain when the AMOC approaches equilibrium again after $\sim$1,000 year. They are separated by a critical value $1 < \alpha_{cr} < 1.5$.

3.1 Effects on subpolar gyre strength

As the CO_2 concentration increases, the warming and strengthened hydrological cycle of the atmosphere lead to increased heat fluxes into (see Fig. 3), and a freshening of (contours in Fig. 4) the ocean, which decrease the surface density of the North Atlantic Ocean.

In the high northern latitudes, the density at the surface is temporarily decreased further by the freshwater flux caused by melting sea ice. Figure 4 illustrates that during the CO_2 increase, surface density is much lower in the supercritical case than in the subcritical case. This situation

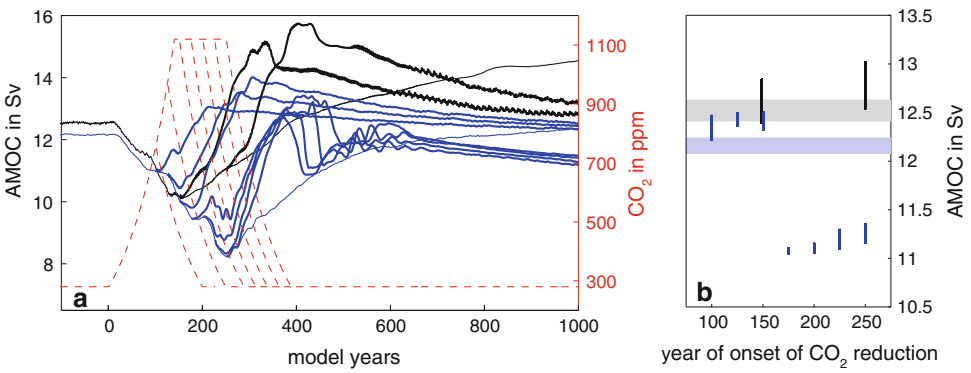

Fig. 2 **a** Time series of the maximum of the overturning stream function in the Atlantic, *black* $\alpha = 1$, *blue* $\alpha = 2$, *thick lines* from the CO_2 peaking experiments, *thin lines* reference from the CO_2 increase experiments (as shown in Fig. 1). *Red*, *dashed line* CO_2 concentrations. **b** Maximum of the overturning stream function in the Atlantic 900–1,000 years after the reduction of the CO_2 concentration was initiated, as a function of the year of the onset of the CO_2 concentration reduction. Colors as in **a**. *Shaded bars* range of the maximum of the equilibrium overturning stream function during years -100 to 0, *grey* $\alpha = 1$, *light blue* $\alpha = 2$

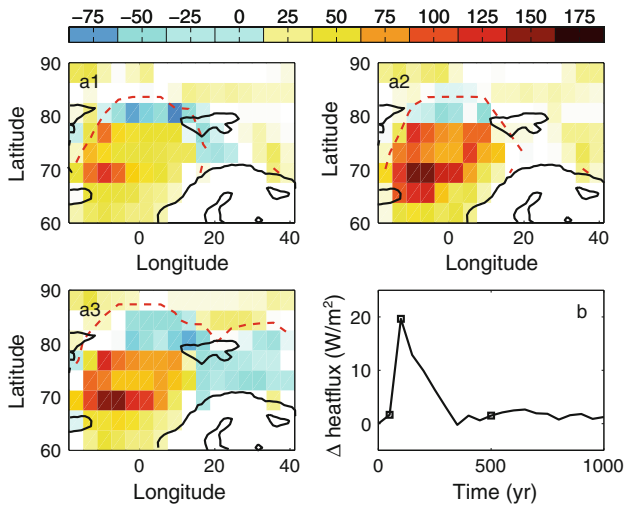

Fig. 3 **a** Maps of the anomaly of the annual mean net heat flux (W m^{-2}) into the ocean for $\alpha = 1$, taken at 50 (**a1**), 100 (**a2**), and 500 (**a3**) years after the start of the CO_2 increase. The *red dashed line* indicates the largest annual extent of 80% sea ice coverage. **b** Time series of the anomaly of the net heat flux (W m^{-2}) into the ocean averaged over the area shown in **a**, *squares* indicate the times of the snapshots shown in **a**

implies higher stratification near the surface, which limits vertical diffusion. The higher the value of α, the stronger is the effect on vertical diffusion (Marzeion et al. 2007).

During the CO_2 increase, the freshwater is therefore more confined to the surface in the supercritical $\alpha = 2$ case than in the subcritical $\alpha = 1$ case (Fig. 4). The weaker downward mixing of freshwater in the supercritical case leads to saltier and denser subsurface waters (100–300 m depth) north of and at the latitude of the GSR, i.e. at the northern rim of the SPG, as seen again in Fig. 4.

The SPG is driven both by the large scale wind pattern and the local density distribution, circulating cyclonically around the dense water in its core, close to geostrophic balance (for a detailed description of the base state of the SPG in the model compare Born et al. 2009). In the supercritical case, the dense anomaly north of and at the latitude of the GSR reduces the meridonal density gradient across the SPG. The reduced meridional density gradient leads to a reduction of the SPG strength (Levermann and Born 2007). This weakening of the SPG is enhanced by the feedbacks described in Levermann and Born (2007). The weakened SPG transports less tropical, saline waters into the subpolar North Atlantic, the center of the SPG freshens, reducing the meridional density gradient and weakening the SPG further. Additionally, the lightening of the center of the SPG implies that fewer isopycnals outcrop in the center of the gyre. This reduces the isopycnal downward mixing of heat within the gyre, resulting in a warming of the SPG, contributing to the light anomaly and weakening of the SPG. Thus, the weak cross-gyre density gradient, as well as the resulting weak geostrophic circulation, are maintained by both temperature and salinity anomalies.

The increasing CO_2 concentrations therefore trigger a separation of the two SPG states that persists after the stabilization of the CO_2 concentration. This separation is due to the link between stratification and vertical mixing introduced by the parametrization employed in the model. The result is a strong warm and fresh anomaly that reduces the density at the center of the SPG in the supercritical case compared to the subcritical case (Fig. 5).

As a consequence, dense water formation in the center of the SPG is more reduced in the supercritical case than in the subcritical case. Figure 6 shows time series of dense water production in the Irminger Sea for all values of α. Towards the end of the CO_2 increase, two different regimes emerge: For small values of α, dense water formation in the Irminger Sea is reduced, but still active. For large values of α, hardly any dense water is being formed in the SPG.

This difference remains as the model approaches the new equilibrium, and corresponds to the difference in the AMOC that is shown in Fig. 5 (contours).

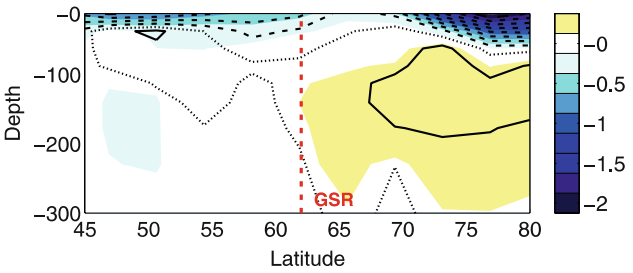

Fig. 4 *Shading* Change in the zonally averaged Atlantic density deviation from the equilibrium ($\Delta\rho$) caused by an increase of α, i.e. $\Delta\rho(\alpha = 2) - \Delta\rho(\alpha = 1)$ in kg m^{-3}, taken at $t = 100$ year. *Contours* Change in the zonally averaged Atlantic salinity deviation from the equilibrium (ΔS) caused by an increase of α, i.e. $\Delta S(\alpha = 2) - \Delta S(\alpha = 1)$ at the same time; *dotted* is zero *contour, dashed* is negative, *solid* is positive. Contour interval 0.3. The *dashed red line* indicates the approximate position of the GSR

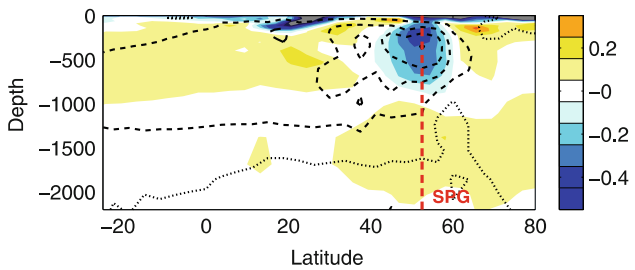

Fig. 5 *Shading* Change in the zonally averaged Atlantic density deviation from the equilibrium ($\Delta\rho$) caused by an increase of α, i.e., $\Delta\rho(\alpha = 2) - \Delta\rho(\alpha = 1)$ in kg m^{-3}, taken at $t = 250$ year. *Contours* Difference of the AMOC streamfunction caused by an increase in α, i.e. $\Psi(\alpha = 2) - \Psi(\alpha = 1)$ at the same time; *dotted* is zero *contour, dashed* is negative. Contour interval 1 Sv. The *dashed red line* indicates the approximate position of the center of the SPG

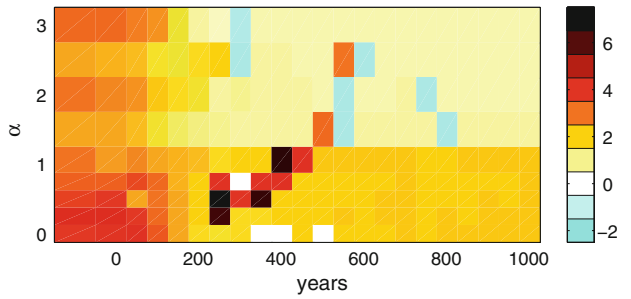

Fig. 6 Rate of dense water production in Sv in the Irminger Sea, as a function of α and time. Dense water formation rates are calculated from annual changes of volume of waters with $\rho \geq 1{,}028$ kg m^{-3}. Note that the values are calculated from annual snapshots, and not averages over each 50 year period. The high rates of dense water formation occuring during the recovery phase are therefore likely to be noise

3.2 The role of sea ice in the recovery of the AMOC

After stabilization of the CO_2 concentration, a recovery of the AMOC sets in for all values of α (Fig. 1). Changes in sea ice cover in the Nordic Seas play an important role for this recovery.

During the CO_2 increase, the high latitude ocean-atmosphere heat flux is reduced by the warmer atmosphere. This leads to a decreased surface density flux into the water, and subsequently decreased dense water formation. Additionally, melting of sea ice contributes to the weakening of the AMOC by adding freshwater to the surface layers. At the same time, however, the melting of sea ice leads to an increase in the area of the ocean surface that is exposed to the atmosphere (Levermann et al. 2007). Figure 3a shows snapshots of heat flux anomalies and ice cover in the Nordic Seas. First, the net heat flux into the ocean increases as the ocean receives more heat from the atmosphere in areas that are not insulated from the atmosphere by sea ice. However, it later decreases in those areas where the sea ice retreats under the influence of the atmospheric warming, and the insulation from the atmosphere is lost. Due to this compensating effect, the heat flux anomalies integrated over the Nordic Seas become very small as the model approaches the new equilibrium under a higher CO_2 concentration (Fig. 3b). As a result, dense water formation and the AMOC north of the GSR recover.

4 Response to the CO_2 peaking scenario

As the atmospheric CO_2 concentration is reduced back to the pre-industrial value, the AMOC recovers (Fig. 2a). As the model approaches the equilibrium state, the recovery is complete for $\alpha = 1$ for both long and short delays of the CO_2 reduction. However, the runs with $\alpha = 2$ only recover to the pre-industrial equilibrium when the reduction is started within 150 years after the increase was started (Fig. 2b). If the reduction of the CO_2 concentration is delayed by 175 years or more, the strong warm and light anomaly of the SPG persists. Indeed, the warming of the SPG is accompanied by a cooling of the Nordic Seas, together leading to a strong reduction of the meridional density gradient across the SPG (Fig. 7). The resulting strong weakening of the SPG is responsible for causing a southeastward recirculation of the warm and salty subtropical waters reaching the north east Atlantic (blue arrows, Fig. 8a). While the inflow into the Nordic Seas only get slightly weaker (Fig. 7), the inflowing water originates rather from the Irminger Sea than from the subtropical Atlantic (Fig. 8a). The reduced inflow of heat into the region leads to reduced heat loss to the atmosphere (Fig. 8b), weakened overturning in the Nordic Seas (Fig. 7), increased ice cover (Fig. 8b), and subsequentally an atmospheric cooling of the northern North Atlantic region (Fig. 9).

5 Discussion and conclusions

Our results indicate that stratification-dependent mixing may lead to a reduction of dense water formation in the SPG that might not be reproduced by ocean models using constant mixing. The recovery of the AMOC that occurs in our model when the CO_2 concentration is stabilized at the fourfold pre-industrial value is associated with changes in sea ice cover in the Nordic Seas.

The warm surface air temperature anomaly due to the increased CO_2 concentration leads to a warming of the surface ocean. As this warm anomaly is penetrating the ocean, it increases the stratification at pycnocline depth. This leads to decreased diffusivities, with the magnitude of

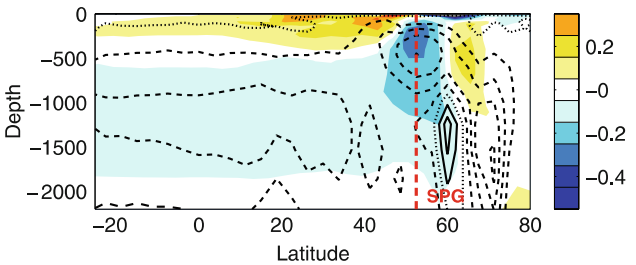

Fig. 7 *Shading* Change in the zonally averaged Atlantic density caused by a delay of the CO_2 reduction for $\alpha = 2$, i.e. $\rho(\alpha = 2$, reduc. 175$)-\rho(\alpha = 2$, reduc. 150$)$, in kg m^{-3}, taken 900 year after the CO_2 concentration reduction started. *Contours* Difference of the AMOC streamfunction caused by a delay of the CO_2 reduction for $\alpha = 2$, i.e. $\Psi(\alpha = 2$, reduc. 175$)-\Psi(\alpha = 2$, reduc. 150$)$, at the same time; *dotted* is zero *contour, dashed* is negative. Contour interval 1 Sv. The *dashed red line* indicates the approximate position of the center of the SPG

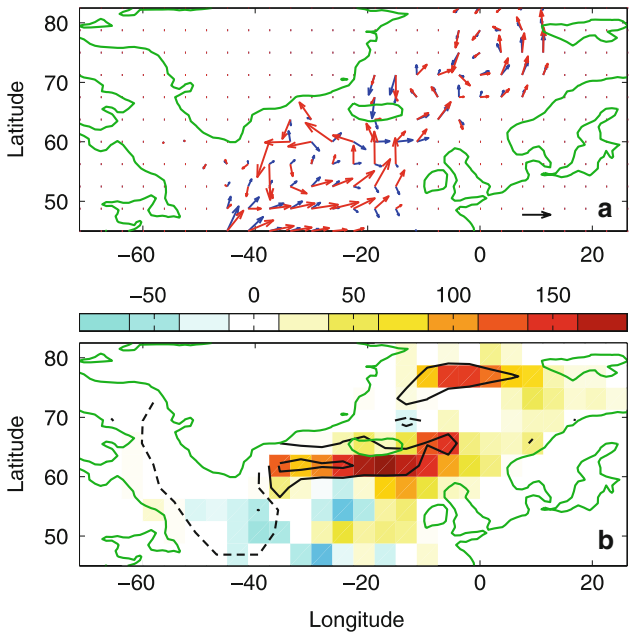

Fig. 8 **a** *Blue arrows* Velocities averaged over the upper 500 m for $\alpha = 2$, reduc. 175. *Red arrows* Velocities averaged over the upper 500 m for $\alpha = 2$, reduc. 150. The *black arrow* in the lower right corner indicates 5 cm s^{-1}. **b** *Shading* Anomaly of the annual mean net heat flux (W m^{-2}) into the ocean caused by a delay of the CO_2 reduction for $\alpha = 2$, taken 900 years after the start of the CO_2 increase. *Contours* Change in the annual mean of percentage sea ice cover caused by a delay of the CO_2 reduction for $\alpha = 2$; *dashed* is zero *contour, solid* is positive. Contour interval 20%

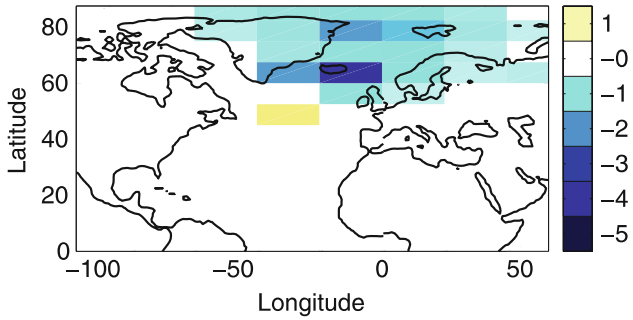

Fig. 9 Change in the annual mean surface air temperature caused by a delay of the CO_2 reduction for $\alpha = 2$, i.e. $T(\alpha = 2$, reduc. 175)−$T(\alpha = 2$, reduc. 150), in K, taken 900 year after the CO_2 concentration reduction started

this effect depending on α. Subsequently, upwelling in low latitudes is weakened, affecting the strength of the AMOC. However, this effect is of second order: Following the estimates of Mignot et al. (2006) for the model used in this study, the observed decrease in low latitude vertical diffusivity accounts for $\sim$0.4 Sv weakening of the AMOC for $\alpha = 1$. This value increases to only $\sim$0.5 Sv for $\alpha = 2$. The weakening and recovery of the AMOC are thus only weakly affected by changes of the diffusivity in the pycnocline in low latitudes that are caused by the mixing parameterization.

Our results further indicate that under stratification-dependent mixing, two different regimes for the North Atlantic ocean circulation exist: One with inflow of warm and saline Atlantic waters into the Nordic Seas, causing a strong heat loss and overturning within the Nordic Seas, as it is presently observed. With a weaker SPG, however, Atlantic waters being advected into the north east Atlantic might recirculate, leading to strongly reduced heat loss to the atmosphere, weakened overturning, and cooling of the Nordic Seas region. While, as in the experiments presented here, a change from one regime to the other could be triggered by an episodic increase of the atmospheric CO_2 concentration, the recirculation regime also occured spontaneously as the equilibrium state in the cases $\alpha = 1.5$ and 2.5, and it has been shown by Levermann and Born (2007) that it can also be triggered by changes to the GSR overflow.

However, our climate model has no atmospheric variability. Given the importance of wind stress forcing to the SPG, it is unclear how a fully coupled model would behave in the experiments presented here. It is nevertheless interesting to note that the modelled SPG undergoes large changes, especially in the peaking CO_2 experiments, without varying wind stress forcing. The nearly complete disappearance of the SPG (see arrows in Fig. 8a) illustrates the importance of the local density distribution for the circulation pattern.

There is no convective mixing in the Labrador Sea in the model used for this study. Instead, all convective mixing occuring south of the GSR is shifted to the Irminger Sea. Our findings illustrate that the changes in dense water formation will likely differ strongly between the regions of deep convection, and might be different if dense water formation was occuring in the Labrador Sea.

While the model does have both spatial and temporal variability in vertical diffusion, we did not account for spatial variability in the energy available for the mixing. Using a parameterization that is equivalent to our $\alpha = 2$ case, Saenko (2006) shows that in an idealized basin setting, the response of the AMOC to increasing CO_2 levels may depend on the spatial distribution of the energy available for mixing. Further work is necessary to include this, and to account for power budget considerations (St. Laurent and Simmons 2006).

The model used for the experiments presented here does not account for increased meltwater run-off following the increasing CO_2 levels. It has been argued that in experiments lacking this feature, the reduced heat fluxes are the dominant effect causing the weakening of the AMOC (Gregory et al. 2005). Also Jungclaus et al. (2006a) suggested that under global warming, the effect of additional

meltwater input from the Greenland ice sheet is small compared to the effect of the changed heat fluxes. The findings presented here however suggest that additional freshening of the high latitude surface ocean might enhance the strength of the feedback between stratification and diffusion, further destabilizing the AMOC, and Swingedouw et al. (2007) found that the additional freshwater input into the North Atlantic caused by increased meltwater run-off may be large enough to cause a permanent shut down of the AMOC.

The model produces excessive concentrations of sea ice in the Barents Sea under pre-industrial conditions (Montoya et al. 2005) which persist at the beginning of the CO_2 increase (Fig. 3a). It is therefore possible that the model overestimates the change in sea ice cover, which would imply that also the recovery of the AMOC is overestimated. Thus, our result that the equilibrium AMOC may be stronger under high concentration of CO_2 needs to be taken with caution.

The experiments presented here can only be a first step in exploring the effect that a more physical parameterization of vertical diffusivity may have on model behavior, and its implications for projections of future climate.

Acknowledgments The comments of two anonymous reviewers helped to improve the manuscript significantly. B. M. was supported under the *GLOMIX* project of the *Research Council of Norway*. A. L. and J. M. were supported by the *Gary Comer Foundation*. This is publication no. A213 from the Bjerknes Centre for Climate Research.

References

Born A, Levermann A, Mignot J (2009) Sensitivity of the Atlantic ocean circulation to a hydraulic overflow parameterisation in a coarse resolution model: response of the subpolar gyre. Ocean Model (published online), doi:10.1016/j.ocemod.2008.11.006

Drange H, Dokken T, Furevik T, Gerdes R, Berger W (eds) (2005) The Nordic seas: an integrated perspective, geophysical monograph series, vol 158. American Geophysical Union, Washington, DC

Fichefet T, Maqueda M (1997) Sensitivity of a global sea ice model on the treatment of ice thermodynamics and dynamics. J Geophys Res 102:12609–12646

Ganachaud A, Wunsch C (2000) Improved estimates of global ocean circulation, heat transport and mixing from hydrographic data. Nature 408:453–456

Gargett AE, Holloway G (1984) Dissipation and diffusion by internal wave breaking. J Mar Res 42:15–27

Gnanadesikan A, Dixon KW, Griffies SM, Balaji V, Barreiro M, Beesley JA, Cooke WF, Delworth TL, Gerdes R, Harrison MJ, Held IM, Hurlin WJ, Lee H, Liang Z, Nong G, Pacanowski RC, Rosati A, Samuels BL, Spelman MJ, Stouffer RJ, Winton M, Wittenberg AT, Dunne JP (2006) GFDL's CM2 global coupled climate models. part II: the baseline ocean simulation. J Clim 19:675–697

Gregory JM, Dixon KW, Stouffer RJ, Weaver AJ, Driesschaert E, Eby M, Fichefet T, Hasumi H, Hu A, Jungclaus JH, Kamenkovich IV, Levermann A, Montoya M, Murakami S, Nawrath S, Oka A, Sokolov AP, Thorpe RB (2005) A model intercomparison of changes in the atlantic thermohaline circulation in response to increasing atmospheric CO_2 concentrations. Geophys Res Lett 32:L12,703. doi:10.1029/2005GL023209

Hall M, Bryden H (1982) Direct estimates and mechanisms of ocean heat transport. Deep-Sea Res 29:339–359

Hátún H, Sandø AB, Drange H, Hansen B, Valdimarsson H (2005) Influence of the Atlantic subpolar gyre on the thermohaline circulation. Science 309:1841–1844

Hátún H, Arge J, Sandø AB (2007) Environmental influence on the spawning distribution and migration pattern of northern blue whiting (Micromesistius poutassou). ICES CM:B06

Hoffert MI, Broecker WS (1978) Apparent vertical eddy diffusion rates in the pycnocline of the Norwegian Sea as determined from the vertical distributium of tritium. Geophys Res Lett 5:502–504

Hofmann M, Maqueda M (2006) Performance of a second-order moments advection scheme in an Ocean general circulation model. J Geophys Res 111:C05,006. doi:10.1029/2005JC003279

Jungclaus JH, Haak H, Esch M, Roeckner E, Marotzke J (2006a) Will Greenland melting halt the thermohaline circulation? Geophys Res Lett 33:L17,708. doi:10.1029/2006GL026815

Jungclaus JH, Keenlyside N, Botzet M, Haak H, Luo J, Latif M, Marotzke J, Mikolajewicz U, Roeckner E (2006b) Ocean circulation and tropical variability in the coupled model ECHAM5/MPI-OM. J Clim 19:3952–3972

Levermann A, Born A (2007) Bistability of the Atlantic subpolar gyre in a coarse resolution climate model. Geophys Res Lett 34:L24,605. doi:10.1029/2007GL031732

Levermann A, Griesel A, Hofmann M, Montoya M, Rahmstorf S (2005) Dynamic sea level changes following changes in the thermohaline circulation. Clim Dyn 24:347–354

Levermann A, Mignot J, Nawrath S, Rahmstorf S (2007) The role of northern sea ice cover for the weakening of the thermohaline circulation under global warming. J Clim 20:4160–4171

Manabe S, Stouffer RJ (1994) Multiple-century response of a coupled ocean-atmosphere model to an increase of atmospheric carbon dioxide. J Clim 7:5–23

Marzeion B, Drange H (2006) Diapycnal mixing in a conceptual model of the Atlantic meridional overturning circulation. Deep-Sea Res II 53:226–238

Marzeion B, Levermann A, Mignot J (2007) The role of stratification-dependent mixing for the stability of the Atlantic overturning in a global climate model. J Phys Oceanogr 37:2672–2681

Mignot J, Levermann A, Griesel A (2006) A decomposition of the Atlantic meridional overturning circulation into physical components using Its sensitivity to vertical diffusivity. J Phys Oceanogr 36:636–650

Montoya M, Griesel A, Levermann A, Mignot J, Hoffmann M, Ganopolski A, Rahmstorf S (2005) The earth system model of intermediate complexity CLIMBER-3α. Part I: description and performance for present day conditions. Clim Dyn 25:237–263

Munk W, Wunsch C (1998) Abyssal recipes II: energetics of tidal and wind mixing. Deep-Sea Res I 45:1977–2010

Nilsson J, Walin G (2001) Freshwater forcing as a booster of the thermohaline circulation. Tellus A 53:629–641

Nilsson J, Broström G, Walin G (2003) The thermohaline circulation and vertical mixing: does weaker density stratification give stronger overturning? J Phys Oceanogr 33:2781–2795

Petoukhov V, Ganopolski A, Brovkin V, Claussen M, Eliseev A, Kubatzki C, Rahmstorf S (2000) CLIMBER 2: a climate system model of intermediate complexity. Part I: model description and performance for present climate. Clim Dyn 16:1–17

Prather MJ (1986) Numerical advection by conservation of second-order moments. J Geophys Res 91:6671–6681

Rahmstorf S, Ganopolski A (1999) Long-term global warming scenarios computed with an efficient coupled climate model. Clim Change 43:353–367

Rehmann CR, Duda TF (2000) Diapycnal diffusivity inferred from scalar microstructure measurements near the New England shelf/slope front. J Phys Oceanogr 30:1354–1371

Saenko OA (2006) The effect of localized mixing on the ocean circulation and time-dependent climate change. J Phys Oceanogr 36:140–160

Sarmiento JL, Feely HW, Moore WS, Bainbridge AE, Broecker WS (1976) The relationship between vertical eddy diffusion and buoyancy gradient in the deep Sea. Earth Plan Sci Lett 32:357–370

St Laurent L, Simmons H (2006) Estimates of power consumed by mixing in the ocean interior. J Clim 19:4877–4890

Swingedouw D, Braconnot P, Delecluse P, Guilyardi E, Marti O (2007) Quantifying the AMOC feedbacks during a 2×CO2 stabilization experiment with land-ice melting. Clim Dyn 29:521–534

Timmermann A, An S, Krebs U, Goosse H (2005) ENSO surpression due to weakening of the North Atlantic thermohaline circulation. J Clim 18:2842–2859

Trenberth KE, Caron JM (2001) Estimates of meridional atmosphere and ocean heat transports. J Clim 14:3433–3443

Vellinga M, Wood RA (2002) Global climatic impacts of a collpase of the Atlantic thermohaline circulation. Clim Change 54:251–267